Signal processing using artificial neural network for BOTDA sensor system

Abul Kalam Azad,[1] Liang Wang,[1,*] Nan Guo,[1] Hwa-Yaw Tam[2] and Chao Lu[1]

[1]*Department of Electronic and Information Engineering, The Hong Kong Polytechnic University, Kowloon, Hong Kong, China*

[2]*Department of Electrical Engineering, The Hong Kong Polytechnic University, Kowloon, Hong Kong, China*

**liangwang@polyu.edu.hk*

Abstract: We experimentally demonstrate the use of artificial neural network (ANN) to process sensing signals obtained from Brillouin optical time domain analyzer (BOTDA). The distributed temperature information is extracted directly from the local Brillouin gain spectra (BGSs) along the fiber under test without the process of determination of Brillouin frequency shift (BFS) and hence conversion from BFS to temperature. Unlike our previous work for short sensing distance where ANN is trained by measured BGSs, here we employ ideal BGSs with different linewidths to train the ANN in order to take the linewidth variation due to different conditions from the training and testing phases into account, making it feasible for long distance sensing. Moreover, the performance of ANN is compared with other two techniques, Lorentzian curve fitting and cross-correlation method, and our results show that ANN has higher accuracy and larger tolerance to measurement error, especially at large frequency scanning step. We also show that the temperature extraction from BOTDA measurements employing ANN is significantly faster than the other two approaches. Hence ANN can be an excellent alternative tool to process BGSs measured by BOTDA and obtain temperature distribution along the fiber, especially when large frequency scanning step is adopted to significantly reduce the measurement time but without sacrifice of sensing accuracy.

OCIS codes: (060.2370) Fiber optics sensors; (290.5900) Scattering, stimulated Brillouin; (070.4340) Nonlinear optical signal processing; (200.4260) Neural networks.

References and links

1. C. A. Galindez-Jamioy and J. M. Lopez-Higuera, "Brillouin Distributed Fiber Sensors: An Overview and Applications," J. of Sensors **204121**, 17 (2012).
2. X. Bao and L. Chen, "Recent Progress in Distributed Fiber Optic Sensors," Sensors (Basel) **12**(12), 8601–8639 (2012).
3. Y. Mizuno, W. Zou, Z. He, and K. Hotate, "Operation of Brillouin optical correlation-domain reflectometry: theoretical analysis and experimental validation," J. Lightwave Technol. **28**(22), 3300–3306 (2010).
4. L. Thévenaz, "Brillouin distributed time-domain sensing in optical fibers: state of the art and perspectives," Front. Optoelectron **3**(1), 13–21 (2010).
5. M. A. Soto, G. Bolognini, F. Di Pasquale, and L. Thévenaz, "Simplex-coded BOTDA fiber sensor with 1 m spatial resolution over a 50 km range," Opt. Lett. **35**(2), 259–261 (2010).
6. C. A. Galindez, A. Quintela, M. A. Quintela, and J. M. Lopez-Higuera, "30cm of spatial resolution using pre-excitation pulse BOTDA technique," Proc. SPIE **7753**, 77531–77534 (2011).
7. Y. Dong, L. Chen, and X. Bao, "Time-division multiplexing-based BOTDA over 100 km sensing length," Opt. Lett. **36**(2), 277–279 (2011).
8. Y. Mao, N. Guo, K. L. Yu, H. Y. Tam, and C. Lu, "1-cm-Spatial-Resolution Brillouin Optical Time-Domain Analysis Based on Bright Pulse Brillouin Gain and Complementary Code," IEEE Ph. J. **4**(6), 2242–2248 (2012).
9. C. N. Pannell, J. Dhliwayo, and D. J. Webb, "The accuracy of parameter estimation from noisy data, with application to resonance peak estimation in distributed Brillouin sensing," Meas. Sci. Technol. **9**(1), 50–57 (1998).
10. C. Zhang, Y. Yang, and A. Li, "Application of Levenberg–Marquardt algorithm in the Brillouin spectrum fitting," Proc. SPIE **7129**, 71291Y (2008).
11. M. A. Soto and L. Thévenaz, "Modeling and evaluating the performance of Brillouin distributed optical fiber sensors," Opt. Express **21**(25), 31347–31366 (2013).

#257807 Received 20 Jan 2016; revised 9 Mar 2016; accepted 9 Mar 2016; published 18 Mar 2016

12. C. Li and Y. Li, "Fitting of Brillouin spectrum based on LabVIEW," in *Proc. 5th Int. Conf. Wireless Commun., Netw. Mobile Comput.* 1–4 Sep. 2009.
13. M. A. Farahani, E. Castillo-Guerra, and B. G. Colpitts, "Accurate estimation of Brillouin frequency shift in Brillouin optical time domain analysis sensors using cross correlation," Opt. Lett. **36**(21), 4275–4277 (2011).
14. M. A. Farahani, E. Castillo-Guerra, and B. G. Colpitts, "A Detailed Evaluation of the Correlation-Based Method Used for Estimation of the Brillouin Frequency Shift in BOTDA Sensors," IEEE Sens. J. **13**(12), 4589–4598 (2013).
15. A. K. Azad, L. Wang, N. Guo, C. Lu, and H. Y. Tam, "Temperature profile extraction using artificial neural network in BOTDA sensor system," in *The 20th Optoelectronics and Communications Conference (OECC), Shanghai, China, Jun. 2015, paper 1570099759.*
16. A. K. Azad, L. Wang, N. Guo, C. Lu, and H. Y. Tam, "Temperature sensing in BOTDA system by using artificial neural network," Electron. Lett. **51**(20), 1578–1580 (2015).
17. R. Ruiz-Lomber, J. M. Serrano, and J. M. Lopez-Higuera, "Automatic strain detection in a Brillouin Optical Time Domain sensor using Principal Component Analysis and Artificial Neural Networks," Sensors (IEEE, 2014), pp. 1539–1542.
18. S. Schlamp, H. G. Hornung, and E. B. Cummings, "Neural network data analysis for laser-induced thermal acoustics," Meas. Sci. Technol. **11**(6), 784–794 (2000).
19. F. N. Khan, Y. Zhou, A. P. T. Lau, and C. Lu, "Modulation format identification in heterogeneous fiber-optic networks using artificial neural networks," Opt. Express **20**(11), 12422–12431 (2012).
20. M. L. Hafiane, Z. Dibi, and O. Manck, "On the Capability of Artificial Neural Networks to Compensate Nonlinearities in Wavelength Sensing," Sensors (Basel) **9**(4), 2884–2894 (2009).
21. K. Abhishek, M. P. Singh, S. Ghosh, and A. Anand, "Weather Forcasting models using Artificial Neural Network," Procedia Tech. **4**, 311–318 (2012).
22. G. Zhang, B. E. Patuwo, and M. Y. Hu, "Forecasting with Artificial Neural Networks: The state of the art," Int. J. Forecast. **14**, 35–62 (1998).
23. A. C. Adrian and L. Ofer, "ANN z: Estimating Photometric Redshifts Using Artificial Neural Networks," Publ. Astron. Soc. Pac. **116**(818), 345–351 (2004).
24. S. Rajasekaran and G. A. V. Pai, *Neural Network, Fuzzy Logic, and Genetic Algorithms - Synthesis and Applications* (Prentice Hall, 2005)
25. D. E. Rumelhart, G. E. Hinton, and R. J. Williams, "Learning representations by back-propagating errors," Nature **323**(6088), 533–536 (1986).
26. J. Li, J. Cheng, J. Shi, and F. Huang, "Brief Introduction of Back Propagation (BP) Neural Network Algorithm and Its Improvements," Proc. AISC169, 553–558 (2012).
27. M. Niklès, L. Thévenaz, and P. A. Robert, "Brillouin gain spectrum characterization in single-mode optical fibers," J. Lightwave Technol. **15**(10), 1842–1851 (1997).
28. X. Bao, A. Brown, M. Demerchant, and J. Smith, "Characterization of the Brillouin-loss spectrum of single-mode fibers by use of very short (<10-ns) pulses," Opt. Lett. **24**(8), 510–512 (1999).

1. Introduction

Distributed fiber optic sensors based on Brillouin scattering have been extensively studied over the past few decades [1–4]. Among them, Brillouin Optical Time Domain Analyzer (BOTDA) sensor systems have been well developed for distributed temperature and strain sensing, which are useful in structural health monitoring, geotechnical engineering and so on [5–8]. In such systems, two counter-propagating signals, pump and probe with different frequencies, interact with an acoustic wave. Due to this interaction, the pump signal transfers part of its energy to the counter-propagating probe signal and the probe signal is amplified. The maximum amplification occurs when the frequency difference of these two signals is exactly equal to the local Brillouin frequency shift (BFS). The local Brillouin gain spectrum (BGS) is obtained by subsequently scanning one of the signal frequencies over the Brillouin gain bandwidth. The BGS obtained at a particular position along the fiber is ideally a Lorentzian-shaped curve and the BFS can simply be determined by finding the central frequency, the frequency with the maximum amplitude of the local BGS [1, 2]. However, the determination of BFS is not such an easy process in practical situations as the spectra obtained from BOTDA measurements are often distorted by noise.

Curve fitting methods, e.g. Lorentzian curve fitting (LCF) and quadratic curve fitting of the measured BGS, are usually adopted to find the BFS [9–12]. In such curve fitting techniques, an ideal curve is fitted onto the measured BGS and the frequency of the maximum amplitude on the fitted BGS is assumed to be the BFS of the measured BGS. However, the curve fitting techniques require the setting of initial parameters and could lead to inaccurate estimation of the BFS, especially if the initializations are too far away from the expected values. The study conducted in [12–14] shows that the accuracy in BFS calculation using LCF

#257807 Received 20 Jan 2016; revised 9 Mar 2016; accepted 9 Mar 2016; published 18 Mar 2016

depends on the proper setting of initial parameters. Moreover, the time needed to process BOTDA sensing signal after data acquisition using curve fitting techniques is relatively long, especially for long sensing range. If frequency scanning step used in BOTDA is increased to reduce the measurement time and processing time, the curve fitting methods provides poor estimation and affects the accuracy due to less data points used for fitting.

In [13, 14], the authors proposed a quite simple but effective method to estimate the BFS of the measured noisy BGS. The technique performs cross-correlation between a known ideal Lorentzian-shaped BGS and the measured BGS to generate a cross-correlated spectrum. The BFS of the measured spectrum is then determined by subtracting the central frequency of the ideal spectrum from that of the cross-correlated spectrum. Unlike LCF, the method does not include any curve fitting process to determine the BFS and, hence would not suffer from the problem brought by the setting of initial parameters. The most attractive feature of the cross-correlation method (XCM) is that it is less sensitive to noise in the spectrum. However, the frequency scanning step used in the BOTDA measurement limits the accuracy of this method. For instance, if the frequency scanning step used is 2 MHz, the determination of BFS using XCM will introduce an error within the range 0 to 1 MHz. This will, in turn, affect the temperature accuracy significantly, especially at higher frequency scanning steps. One of the possible ways to overcome this limitation is to use very small frequency scanning step during data acquisition so that the temperature accuracy can be maintained to an acceptable value. But the price to be paid for using such small scanning step is the increase in data acquisition time. Alternatively, the acquired data can be up-sampled by using data interpolation technique which, in turns, increases the data processing time. Thus fast monitoring of temperature/strain using this method is limited in areas where large error is acceptable, i.e., in fire detection application [14].

On the other hand, artificial neural network (ANN) has been widely employed for different applications of estimation in science and engineering to achieve complex input-output relationship as well as nonlinear mapping ability in recent years [15–23]. It outperforms other conventional nonlinear methods since it does not require much prior input-output relationships on the nature of nonlinearity existing between the input and output patterns [21, 22]. Therefore, it is inherently much more flexible for practical implementation. Since the BGS is a nonlinear curve, and the estimation of BFS and temperature from the BGS is also a nonlinear process, the nonlinear mapping capability of ANN can be well used to extract temperature information from the BGSs along the fiber. Previously, we have proposed the use of ANN to extract the temperature information directly from the BGSs measured by BOTDA system [15, 16]. No curve fitting process is needed, and the process of determination of BFS and conversion from BFS to temperature are also not required. Since ANN is trained and optimized to acquire the knowledge about the pattern of the BGSs and corresponding temperatures before it is used for temperature extraction, it can offer better accuracy and larger tolerance to error even if large frequency scanning step is adopted to reduce the measurement time. In this paper, instead of the very short sensing distance demonstrated in Ref [15, 16], we have demonstrated the use of ANN in BOTDA system for sensing in the range of 41 km by employing ideal BGSs with different linewidths to train the ANN and hence to minimize the effect of BGS linewidth variation along FUT on the ANN performance. We find that at large frequency scanning step, the performance of BOTDA with ANN for temperature extraction does not degrade significantly. By comparison of the ANN performance with that of curve fitting technique (e.g. LCF) and XCM, our results show that ANN can provide higher accuracy, greater tolerance to the measurement error and faster data processing speed, especially when large frequency scanning step is adopted for data acquisition. The use of ANN can help to reduce the measurement time greatly by adopting large frequency scanning step in BOTDA system, but without much sacrifice of the sensing accuracy.

#257807 Received 20 Jan 2016; revised 9 Mar 2016; accepted 9 Mar 2016; published 18 Mar 2016

2. BOTDA experiment setup

The experiment setup of the BOTDA sensing system is shown in Fig. 1. The output of a CW tunable laser operating at 1550 nm is split into two branches using a 20/80 coupler. The CW signal at the upper branch is modulated by an electro-optic modulator (EOM1) to generate 40 ns pump pulse which corresponds to a spatial resolution of 4 m. An erbium-doped fiber amplifier (EDFA) is then used to increase the peak pump power before the pulse enters the fiber under test (FUT). A polarization scrambler (PS) is used to suppress the polarization dependent noise. The signal at the lower branch is modulated by another EOM2 biased at Null

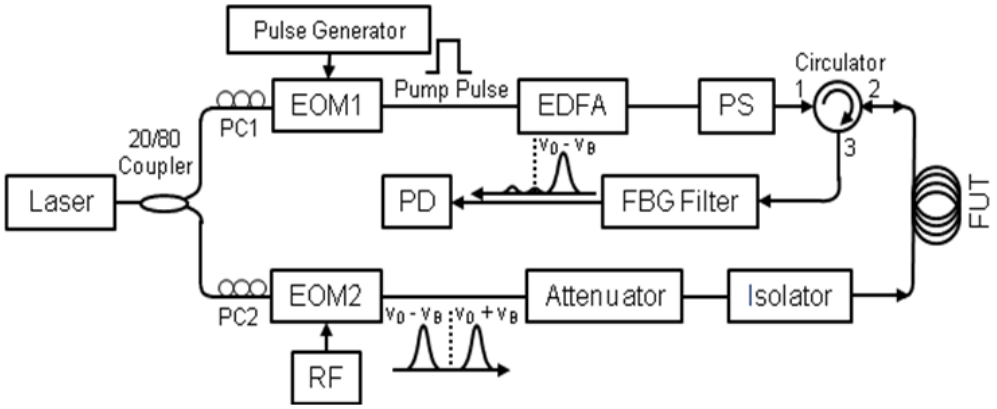

Fig. 1. BOTDA experiment setup, PC: Polarization Controller, EOM: Electro-Optic Modulator, RF: Radio Frequency, EDFA: Erbium-doped Fiber Amplifier, PS: Polarization Scrambler, PD: Photodetector, FBG: Fiber Bragg Grating, FUT: Fiber under test.

point to suppress the optical carrier and driven at a frequency around BFS. A variable optical attenuator is used to control the probe power and the isolator followed blocks the signal from the reverse direction. The probe signal is detected by a photodetector after the unwanted sideband is filtered out by a fiber Bragg grating (FBG). The local BGS is obtained by scanning the frequency of the probe signal in the vicinity of BFS. In order to examine the performance of ANN when using large frequency scanning steps, the BGSs are collected using several frequency scanning steps, e.g. 1, 2, 5, 10, 15 and 20 MHz. The frequency scanning range is from 10.75 GHz to 10.95 GHz and 2000 times averaging of the traces are adopted. Then the collected data are processed and temperature information is extracted by ANN and, also by LCF and XCM for comparison.

3. Operating principle of temperature extraction using ANN, LCF and XCM

3.1 Artificial neural network (ANN)

An ANN is a simplified computational model comprised of several layers of interconnected neurons. Figure 2 shows a typical ANN with input and output layers together with one hidden layer, which are interconnected with different weights. The use of ANN for input-output mapping problems involves two independent phases. One is the training phase where the connecting weights between the neurons of two adjacent layers are optimized for known input-output patterns. The other one is the testing phase where the ANN with optimized

#257807 Received 20 Jan 2016; revised 9 Mar 2016; accepted 9 Mar 2016; published 18 Mar 2016

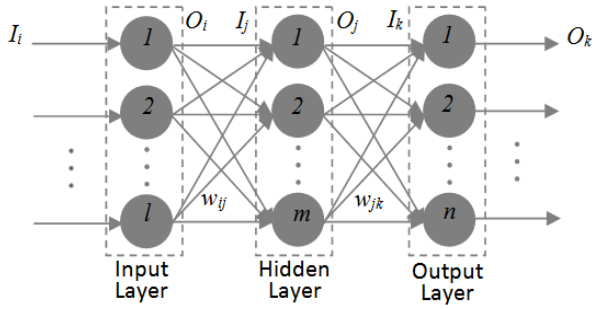

Fig. 2. A typical feed-forward artificial neural network (ANN) with one hidden layer.

weights is used to determine the output patterns for the given input patterns. The training of ANN is realized via back-propagation (BP) learning algorithm [24–26], where the random initial weights are updated until a desired mean square error (MSE) between the known output patterns and those determined by ANN is satisfied. After the optimization of weights among neurons of different layers, ANN is reconfigured and ready to produce outputs for testing input patterns in the testing phase. The number of hidden layer(s) and that of neurons in each hidden layer as well as the tuning parameters of BP algorithm are usually adjusted based on empirical trial and error performance. However, it is not difficult to adjust these parameters in order to obtain the satisfactory results [18]. Since the training and testing phases of ANN are fully independent, ANN can provide output very fast once it is trained.

To extract temperature profile from the BGSs measured by BOTDA, a multilayer feed-forward ANN is used. The training and testing phases of the ANN for extracting temperature information from the BGSs is shown in Fig. 3. In the training phase, the BGS under one temperature (T) together with this temperature constitute one input-output pattern for ANN training. And a number of such BGS-T pairs are used as input-output patterns to train the ANN. Note the BGS at each T is normalized. The weights of ANN are then updated and optimized by BP algorithm. Once the training is completed, the weights connecting the neurons of different layers are optimized and the ANN is ready for temperature extraction. In the testing phase, the measured BGSs along FUT by BOTDA are fed to the input layer of ANN. The output layer of ANN with optimized weights produce the temperature distribution along the FUT directly without the process of determination of BFS, and hence conversion from BFS to temperature.

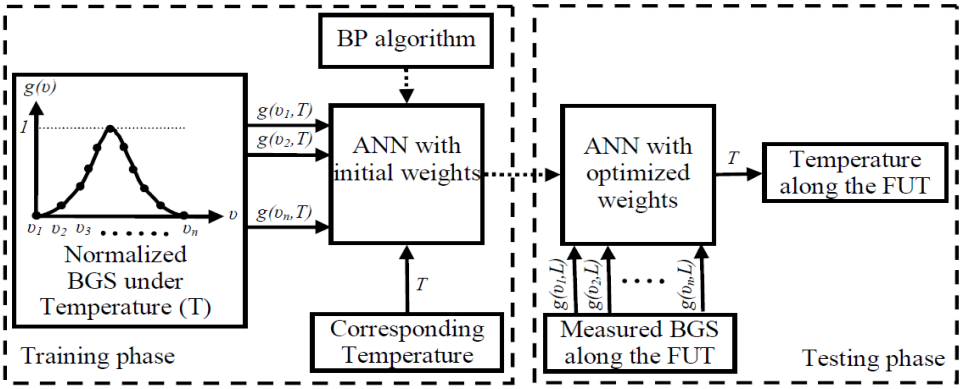

Fig. 3. Two independent phases in using ANN to extract temperature information from BGSs.

Before applying ANN to temperature extraction, we need BGS-T pairs as the known input-output patterns to train the ANN. To get the BGS-T pairs, we put a short fiber of about 100 m long into the oven, and measure the BGS distribution along the fiber using the setup in Fig. 1. The frequency scanning range is from 10.75 GHz to 10.95 GHz with 1MHz scanning

#257807 Received 20 Jan 2016; revised 9 Mar 2016; accepted 9 Mar 2016; published 18 Mar 2016

step and 2000 times averaging of the trace is adopted. The BGS for each fiber location is normalized and then the normalized BGSs along the fiber are all averaged to obtain one averaged BGS. The averaged BGS together with the temperature set in the oven serves as one BGS-T pair. The temperature of the oven is changed from room temperature (~21 °C) to 65 °C with a step of ~1°C. Thus we can get 45 BGS-T pairs as the known input-output patterns for ANN training. Figure 4(a) shows the 45 BGS-T pairs. The variation of BFS with temperature is also shown in Fig. 4(b), where the BFS varies linearly with temperature with a slope of ~0.92924 MHz/°C and the BFS at 25 °C is found to be 10.82891 GHz.

The averaged BGSs shown in Fig. 4(a) together with their corresponding temperatures can directly be used to train the ANN for extracting temperature information along the fiber as long as the training and testing BGSs are obtained from BOTDA measurements under the same condition [15,16]. And to ensure the exact temperature extraction, the linewidth of the training and testing BGSs should be ideally the same. However, the training and testing BGSs

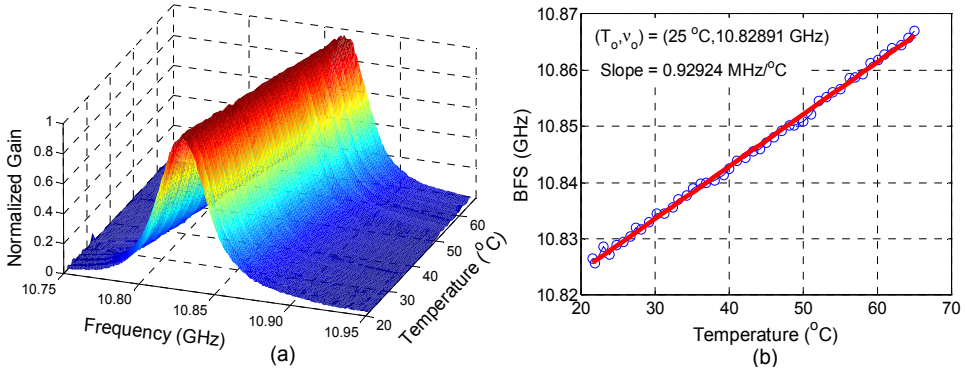

Fig. 4. (a) Averaged BGS for room temperature (~21 °C) to 65 °C and (b) BFS vs temperature.

are generally obtained from different experiment measurements and conditions, thus, the linewidth of BGSs may vary due to various factors [27, 28]. Since the ANN for temperature extraction is based on the knowledge it acquires during training process, its performance will greatly be affected if the linewidth of the training and testing BGSs is not matched. One way to solve this problem is to measure all the BGSs along the FUT at different temperatures for training as described above, but it is only practical for short sensing fiber [15, 16]. While for long distance sensing, to minimize the effect of linewidth variation on the ANN performance, we train the ANN by using ideal BGSs with different linewidth instead of using those shown in Fig. 4(a). In the experiment, we adopt pump pulse of duration 40 ns which is much longer than the phonon life time (~10 ns). The BGSs obtained from BOTDA measurements for using such pump pulse can be modeled by Lorentzian profile [28]. Thus the ideal BGSs for the training of ANN are obtained using the Lorentzian gain spectrum given by Eq. (1), where

$$g(\upsilon) = \frac{g_B}{1+[(\upsilon-\upsilon_B)/(\Delta\upsilon_B/2)]^2} \tag{1}$$

ν_B is the BFS, $\Delta\nu_B$ is the linewidth and g_B is the peak gain of the spectrum. The BFSs of the ideal BGSs are determined using the temperature coefficient (slope) and the value of BFS at 25 °C in Fig. 4(b), from a temperature range of 10 °C to 70 °C with 1 °C step. And for each temperature, we have several BGSs of the same BFS but with different linewidth varying from 25 to 70 MHz at a step of 1 MHz. The range of linewidth is chosen considering the practical variation of BGS linewidth usually obtained from BOTDA measurements. In such a way, we have 61 × 46 ideal BGS-T pairs for ANN training. The frequency range in Eq. (1) is from 10.75 GHz to 10.95 GHz, the same as the frequency scanning range in the experiment. Similarly six frequency steps (1, 2, 5, 10, 15 and 20 MHz) in obtaining the ideal BGSs are used and for each frequency step we can obtain one trained ANN to extract the temperature

#257807 Received 20 Jan 2016; revised 9 Mar 2016; accepted 9 Mar 2016; published 18 Mar 2016

from the measured BGSs with the corresponding frequency scanning step. The reason for using ideal BGSs to train the ANN is that it is very difficult to obtain the BGSs with variable linewidth from experiment to represent all the conditions. The ideal BGSs and their corresponding temperatures used to train the ANN are normalized to have values between 0 and 1. This is because the ANN works better with normalized data [22, 24]. In addition, we use linear transfer function for the neurons in input layer but sigmoid transfer function for that of both in hidden and output layers, and sigmoid function can only have output values between 0 and 1. Then after training using the ideal BGSs, six ANNs with optimized weights are used to extract the temperature information from the measured BGSs for six frequency scanning steps, respectively. For the ANN under each frequency scanning step, the number of neurons in the input layer is equal to the number of data samples on the measured BGSs obtained at that frequency scanning step, while the output layer consists of only 1 neuron representing the corresponding temperature output. It should be mentioned that during the training phase, an extra bias neuron is added to the input layer of ANN to improve the mapping process [23, 24]. The value of the bias neuron is constantly set to '1'. With respect to the number of hidden layers, one hidden layer could be enough for most of the situations, while two hidden layers may give better results for the case where one hidden layer is filled with too many neurons to give satisfactory results [22]. In this study, we have observed that the training of two-hidden-layer ANN can give acceptable performance when the number of data samples on the BGS is relatively large. Thus we have used two-hidden-layer ANN for 1, 2, and 5 MHz frequency steps, but one -hidden-layer ANN for 10, 15 and 20 MHz steps. Also there is no general guideline to determine the number of neurons in the hidden layer, and the most common way is based on experiments or by trial-and-error [22]. We have also considered a number of combinations of neurons in the hidden layers. With numerous trials, the layout of the ANNs in both the training and testing phases are finalized to be 202-50-7-1, 102-40-6-1, 42-10-4-1, 22-22-1, 15-15-1 and 12-12-1, used for 1, 2, 5, 10, 15 and 20 MHz frequency scanning steps respectively, where the numbers separated by dash (-) represent the number of neurons in each layer starting from the input layer and ending at the output layer. Since we have not tried all possible combinations, the ANNs used in our study may not be the best possible choice but still they can provide satisfactory results.

3.2 Lorentzian curve fitting (LCF)

In theory, the Brillouin gain spectrum (BGS) obtained from BOTDA measurement is ideally modeled by a Lorentzian curve and the spectrum are defined by three parameters given by Eq. (1) [1, 2]. Among the three parameters, the most important one for temperature/strain sensing applications is the BFS (ν_B) along the fiber which varies linearly with temperature (T) and strain (ε) as expressed in Eq. (2) [1]. In Eq. (2), C_T and C_ε are the temperature and strain

$$\upsilon_B(T,\varepsilon) = C_T \Delta T + C_\varepsilon \Delta\varepsilon + \upsilon_B(T_o,\varepsilon_o) \tag{2}$$

coefficients respectively. In LCF technique, the ideal Lorentzian curve is fitted onto the measured spectrum and BFS of the measured spectrum is assumed to be the frequency with maximum amplitude on the fitted curve. The BFS is then converted to temperature using Eq. (2). To perform LCF, nonlinear least squares estimation (LSE) with Levenberg-Marquardt (LM) algorithm is adopted in this paper. With this algorithm, the vector $\mathbf{p} = (g_B, \nu_B, \Delta\nu_B)$ containing the three model parameters in Eq. (1) is updated in each iterations until the best agreement between the data and model is achieved by minimizing the objective function given by Eq. (3). In Eq. (3), $g(\nu_i)$ is the measured data and $g(\nu_i, \mathbf{p})$ is the fitted data. The initial

$$\sum_{i=1}^{N}[g(\upsilon_i) - g(\upsilon_i, \mathbf{P})]^2 \tag{3}$$

parameters are usually chosen from the underlying curve described in [13, 14]. However, the accuracy of BFS estimation using this technique depends on the choice of initial parameters

#257807 Received 20 Jan 2016; revised 9 Mar 2016; accepted 9 Mar 2016; published 18 Mar 2016

[12–14]. As an example, an unknown noisy Lorentzian spectrum, $g_u(\nu)$ and its Lorentzian fitted curve, $g_L(\nu)$ obtained by such LCF technique is shown in Fig. 5.

3.3 Cross-correlation method (XCM)

The XCM is based on the fact that the cross-correlation between a reference ideal Lorentzian spectrum and an unknown noisy Lorentzian spectrum results in another Lorentzian curve [13, 14]. The central frequency and linewidth of the resultant spectrum is equal to the sum of central frequencies and linewidths of the two spectra used for cross-correlation. The central frequency of the resultant spectrum is determined simply by finding the frequency with maximum amplitude. Thus the central frequency of the unknown noisy spectrum can simply be determined by subtracting the central frequency of the reference ideal spectrum from that of the cross-correlated spectrum. The BFS of the unknown spectrum is then converted to temperature with the linear relationship given by Eq. (2). For example, the XCM operation is graphically illustrated in Fig. 5 for the same unknown spectrum $g_u(\nu)$ used in LCF technique. The reference ideal spectrum, $g_r(\nu)$ is obtained by Eq. (1) whose peak gain, central frequency and linewidth are known. The cross-correlation between $g_u(\nu)$ and $g_r(\nu)$ produces $g_c(\nu)$ which

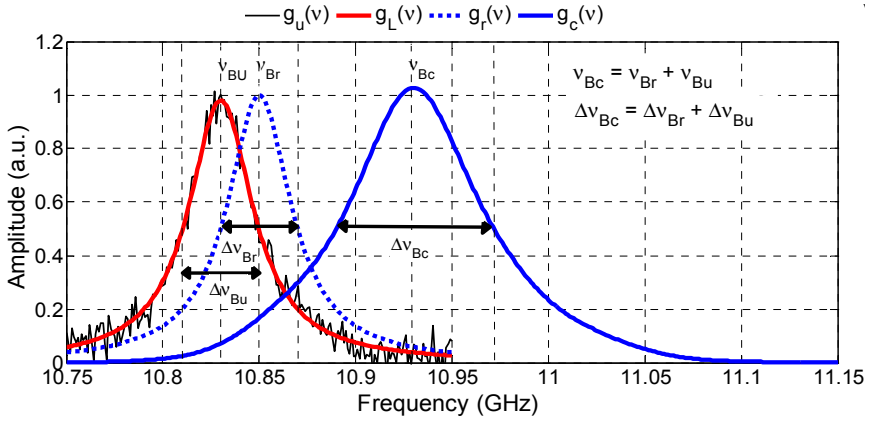

Fig. 5. Illustration of LCF and XCM. $g_u(\nu)$ is an unknown noisy spectrum and $g_L(\nu)$ is fitted by LCF technique. $g_r(\nu)$ is an ideal Lorentzian curve and $g_c(\nu)$ is obtained by cross-correlating $g_r(\nu)$ and $g_u(\nu)$.

is also a Lorentzian curve. The most important feature of $g_c(\nu)$ is that its shape is mainly determined by the signal rather than the noise. Even if the noisy curve is an imperfect Lorentzian (worst-case Gaussian) curve, the cross-correlated spectrum has Lorentzian distribution around the peak area which is actually the area of interest for Brillouin sensing applications [14]. Note that in Fig. 5 the amplitude of $g_c(\nu)$ is scaled down by a factor of 30 in order to accommodate all the spectra in the same plot.

4. Experimental results and discussion

In the experiment, a FUT of 41 km long is used in the BOTDA setup shown in Fig. 1. The last 50 m of the FUT is put into the oven which is set at several different temperatures: room temperature (~21 °C), 29.90 °C, 39.14 °C and 48.63 °C during each experiment. The 3- D distribution of the BGSs acquired for the temperature of 39.14 °C at 1MHz frequency scanning step is shown in Fig. 6(a). The corresponding BOTDA trace along the fiber at 10.84 GHz is shown in Fig. 6(b) from which it can be easily observed that the spatial resolution of the system is ~4 m. It is worth mentioning that the noisy trace may be due to the uneven strain distribution along the FUT compactly wound on to the mandrel.

#257807 Received 20 Jan 2016; revised 9 Mar 2016; accepted 9 Mar 2016; published 18 Mar 2016

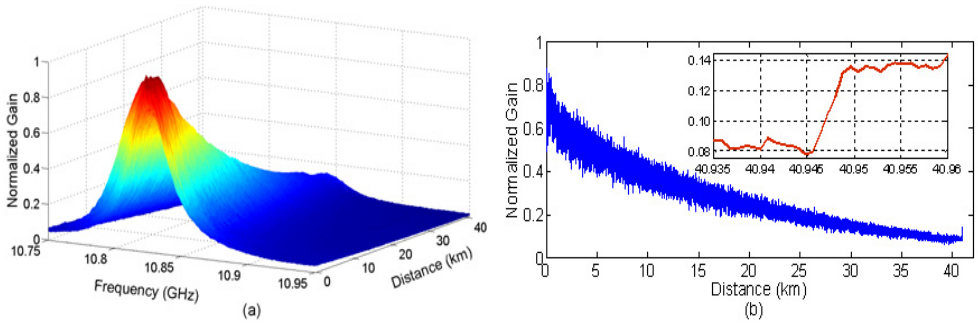

Fig. 6. (a) Normalized BGS along 41 km fiber with the last 50 m heated at 39.14 °C. The frequency scanning step is 1 MHz. (b) The BOTDA trace obtained at 10.84 GHz along the fiber. The inset shows the spatial resolution of ~4 m.

To extract temperature information from the BGSs along the FUT, six trained ANNs suitable for six frequency scanning steps are obtained after the training phase. In the testing phase, the trained ANN with optimized weights is employed to directly extract temperature information from the BGSs obtained at that scanning step. The BGSs fed to the ANN during testing phase are also normalized like that in training phase by making the peak gain of each spectrum along FUT equal to 1. The extracted temperature distributions by ANNs for all of the four different temperatures at different frequency scanning steps are shown in Fig. 7. The results show that ANN can be successfully used to extract temperature information along the FUT even at large frequency scanning steps, in which the maximum frequency step adopted (20 MHz) is approximately within the half of the linewidth of the BGS (~40 MHz). The temperature distributions obtained at different frequency steps are almost similar and the performance of ANN at such large frequency scanning steps is comparable with that at small frequency steps. It can be easily observed from Fig. 7 that the performance of ANN does not degrade significantly at different higher frequency scanning steps up to 20 MHz. This is because ANN is trained and optimized to acquire the knowledge about the pattern of the BGSs and corresponding temperatures for each frequency scanning step separately before it is used for temperature extraction. Hence the measurement time of BOTDA system with ANN for temperature extraction could be possibly reduced by adopting certain large frequency scanning step depending on the linewidths of the BGSs but without sacrificing accuracy significantly.

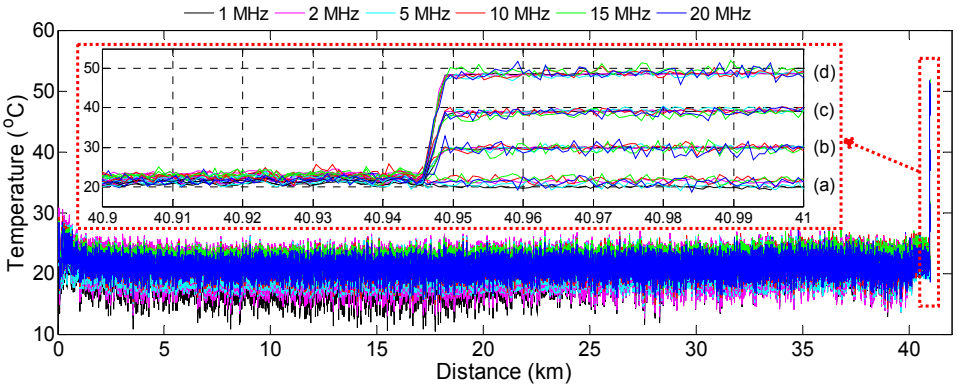

Fig. 7. ANN determined temperature distribution along 41 km long FUT whose last 50 m is heated at (a) room temperature (~21 °C), (b) 29.90°C, (c) 39.14°C and (d) 48.63 °C; inset: temperature distribution within a range of last 100m from 40.9 km to 41 km.

Next we compare the results by ANN with those by LCF or XCM. The ANN can extract the temperature information from the BGSs directly without the process of determination of BFS, and hence conversion from BFS to temperature. While in using LCF or XCM, the BFS

#257807 Received 20 Jan 2016; revised 9 Mar 2016; accepted 9 Mar 2016; published 18 Mar 2016

is first determined from the BGSs and then the temperature information along the FUT is calculated based on the linear relationship given by Eq. (2). The results obtained by LCF and XCM are shown in Fig. 8 and Fig. 9 respectively. It should be mentioned that for XCM, to improve the accuracy to an acceptable level, the BGSs obtained from BOTDA measurements are up-sampled using data interpolation technique before applying cross-correlation. As the frequency scanning step increases, the fluctuation of the temperature distribution along the FUT using both LCF and XCM become larger, unlike the results by ANN in Fig. 7. Moreover, the value of measured temperatures obtained at large frequency scanning steps becomes larger compared to that obtained at small scanning steps; while the measured temperature obtained at different scanning steps is almost the same by using ANN. Thus the temperature error using both LCF and XCM increases largely when the frequency scanning step is increased. Since the width of BGS is around 40 MHz, with the frequency scanning step increasing, fewer data points appear on the measured BGS, especially when the scanning step is half of the BGS linewidth (20 MHz). Thus the performance of using LCF and XCM in Fig. 8 and Fig. 9 degrades significantly because there are fewer data points used for retrieving the temperature at large frequency scanning step. While the ANN performance does not degrade significantly as compared to LCF and XCM, because the ANNs are trained to learn about the patterns of the BGSs and corresponding temperatures for each frequency step separately before it is used for temperature extraction. This is more obvious in the following analysis.

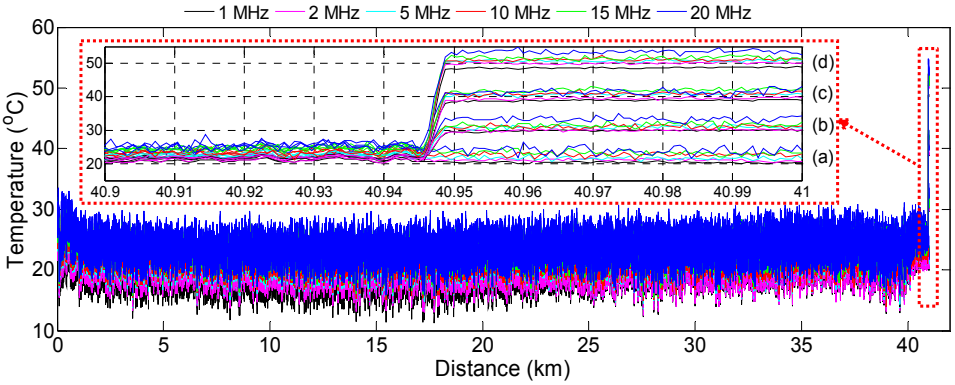

Fig. 8. LCF determined temperature distribution along 41 km long FUT whose last 50 m is heated at (a) room temperature (~21 °C), (b) 29.90°C, (c) 39.14°C and (d) 48.63 °C; inset: temperature distribution within a range of last 100m from 40.9 km to 41 km.

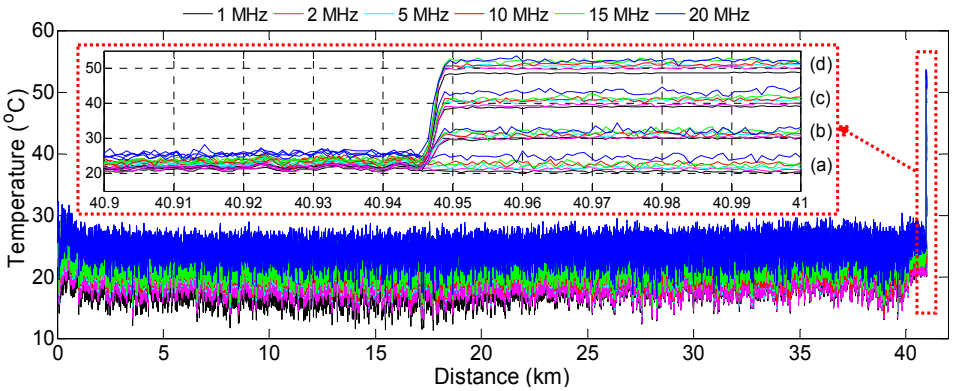

Fig. 9. XCM determined temperature distribution along 41 km long FUT whose last 50 m is heated at (a) room temperature (~21 °C), (b) 29.90°C, (c) 39.14°C and (d) 48.63 °C; inset: temperature distribution within a range of last 100m from 40.9 km to 41 km.

#257807 Received 20 Jan 2016; revised 9 Mar 2016; accepted 9 Mar 2016; published 18 Mar 2016

In order to evaluate the error performance of ANN, LCF and XCM, we calculate the absolute temperature error distribution along the last 50 m FUT. The absolute temperature error is defined as the absolute difference between the temperature (T_m) measured by thermometer and the one (T_c) extracted by ANN or LCF or XCM. The results are given in Fig. 10, Fig. 11 and Fig. 12 for three different temperatures: 29.90 °C, 39.14 °C and 48.63 °C respectively. From the three figures, we can see that at small scanning steps, e.g. 1 MHz, due to sufficient number of data points on the measured BGSs, the AE distributions by ANN, LCF and XCM are comparable and all of them are very close to 0. Although the fluctuation of the AE distributions using all of these methods increases as the frequency scanning step increases, the AE using ANN at large scanning steps shows an average value more close to

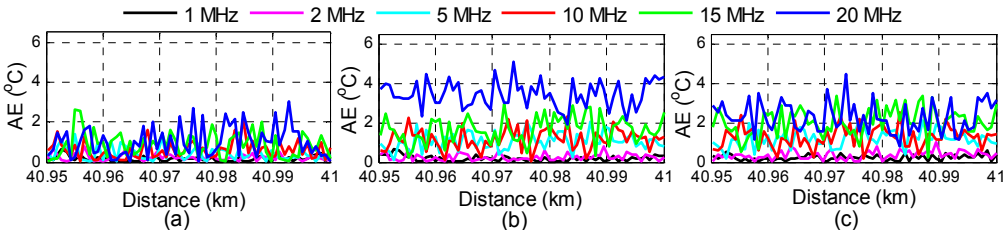

Fig. 10. Absolute Error distribution along the last 50 m FUT calculated using (a) ANN, (b) LCF and (c) XCM for a temperature of 29.90 °C.

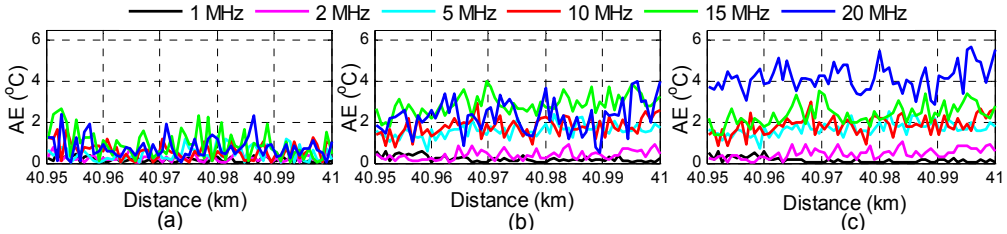

Fig. 11. Absolute Error distribution along the last 50 m FUT calculated using (a) ANN, (b) LCF and (c) XCM for a temperature of 39.14 °C.

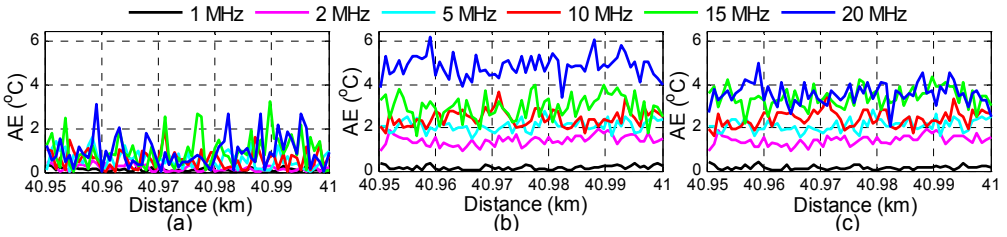

Fig. 12. Absolute Error distribution along the last 50 m FUT calculated using (a) ANN, (b) LCF and (c) XCM for a temperature of 48.63 °C.

zero, unlike those using LCF or XCM become far away from zero. Under a certain BGS width of 40 MHz, fewer data points are obtained on the measured BGS at large frequency scanning steps, leading to performance degradation of temperature extraction by LCF or XCM. While at larger frequency scanning steps ANN can provide more accurate temperature measurement and again confirms the superiority of ANN over LCF and XCM at large frequency steps. We also compare the performance of ANN, LCF, and XCM in terms of root mean square error (RMSE) at different frequency scanning steps. The RMSE is calculated using the temperatures (T_m) measured by thermometer and that determined by ANN, LCF and XCM, respectively along the last 50 m fiber. The results are shown in Fig. 13. It is observed from the results that at each frequency scanning step, the ANN provides smaller RMSE than

#257807 Received 20 Jan 2016; revised 9 Mar 2016; accepted 9 Mar 2016; published 18 Mar 2016

both LCF and XCM, which means the measured temperatures using ANN, are more close to T_m and hence ANN offers better accuracy. As the frequency step increases, we see that both the RMSE using LCF and XCM degrades much more quickly than that using ANN. Taking the

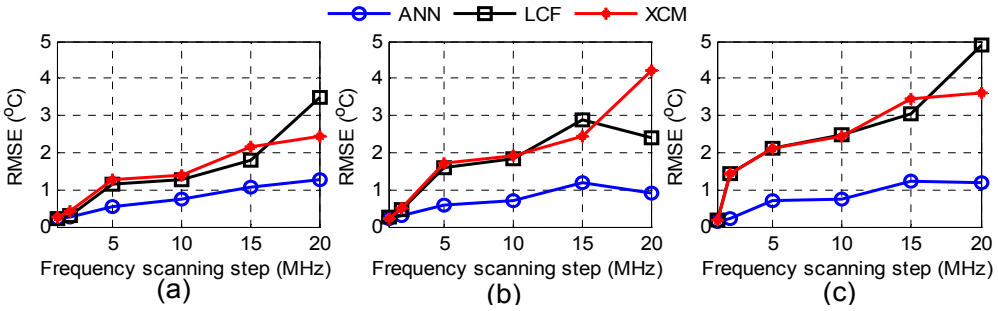

Fig. 13. RMSE for the last 50 m fiber heated to (a) 29.90 °C, (b) 39.14 °C and (c) 48.63 °C. At each frequency scanning step, the measured temperatures are obtained using ANN, LCF and XCM, respectively.

case of 39.14 °C as an example, the RMSE using ANN at 15 MHz scanning step is 1.172 °C, which is even smaller than RMSE of 1.608 °C using LCF and 1.705 °C using XCM at 5 MHz scanning step. This is also true in the cases of the other two temperatures. This implies that temperature extraction using ANN at large scanning step, e.g. 15 MHz, has better performance than that using LCF and XCM at small scanning step, e.g. 5 MHz. In other words, ANN can adopt large scanning step up to a certain value depending on the linewidth of BGS (half of the BGS linewidth in our case) for temperature extraction to achieve comparable performance as those adopting small scanning step using LCF or XCM. As a result, the data acquisition time by BOTDA measurement can be greatly reduced with large frequency scanning step but without sacrificing much accuracy if ANN is used for temperature extraction and the accuracy at such scanning step is acceptable in practical situations. It should be mentioned that the fluctuations of RMSEs in Fig. 13(a), 13(b) and 13(c) for using LCF and XCM, especially at large frequency steps are due to the uneven distributions of data points on the measured BGSs around the peak area. In addition, the RMSEs for using both LCF and XCM are observed to increase as the fiber temperature increases, which may originate from the fact that the linewidth of the BGSs decreases when the fiber temperature increases [27], resulting in the number of data points near the peak area of the BGS to become a little smaller accordingly. However, for extracting temperature information from the BGSs obtained at different frequency steps, the ANNs are trained separately and the effect of linewidth variation of the measured BGSs on ANN performance is compensated. Thus the linewidth variation of measured BGSs does not affect the performance of ANNs significantly and they give almost similar results at a particular scanning step for fiber temperatures of 29.90 °C, 39.14 °C and 48.63 °C as shown in Fig. 13(a), 13(b) and 13(c). The performance of ANNs degrades at large frequency scanning step due to small number of data points near the peak area of the BGSs but the degradation is much less than those using LCF and XCM. From Fig. 13 we can see that the ANN has better accuracy and larger tolerance to error compared to LCF and XCM, which is because ANN is trained and optimized to acquire the knowledge about the pattern of the BGSs and corresponding temperatures for each frequency scanning step separately before it is used for temperature extraction. To confirm the superiority of ANN more clearly, standard deviation (SD) of the temperature distribution along the FUT using ANN, LCF and XCM is calculated. For the comparison, SD is calculated near the end of the FUT where the signal-to-noise ratio (SNR) is the worst. Figure 14(a) shows the SD of the temperature distribution computed for every 50 m from 39 to 40 km for the case of 1 MHz frequency scanning step. Figure 14(b) compares the SD calculated within the range from

#257807 Received 20 Jan 2016; revised 9 Mar 2016; accepted 9 Mar 2016; published 18 Mar 2016

39.95 to 40 km at different frequency scanning steps. At small frequency scanning step, the performance using ANN, LCF and XCM is almost the same, which is implied in Fig. 14(a)

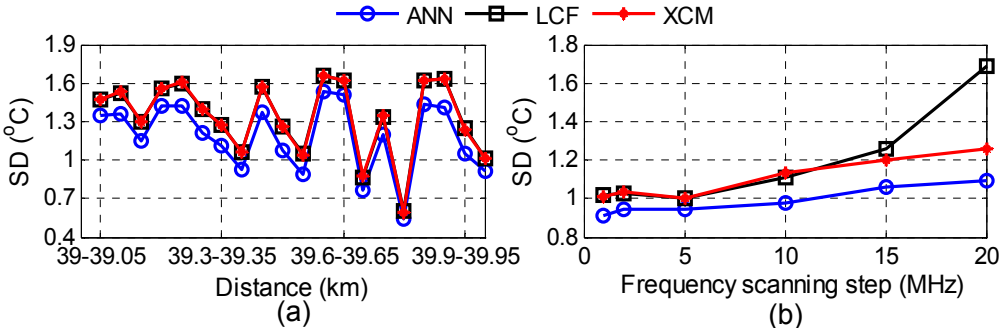

Fig. 14. Standard deviation (SD) along the fiber computed within (a) every 50 m from 39 km to 40 km for the case of 1 MHz frequency scanning step, and (b) 50 m from 39.95 km to 40 km for cases of different frequency scanning steps.

where the SD using ANN is comparable to those using LCF and XCM, But for scanning steps beyond 1 MHz, the SD using ANN becomes better than those using LCF and XCM, especially at large scanning step, as shown in Fig. 14(b). For instance, at 10 MHz scanning step, the SD using ANN, LCF and XCM are 0.975 °C, 1.114 °C, and 1.136 °C respectively. Figure 14 again confirms the superiority of ANN approach over LCF and XCM methods when adopting larger scanning step. It is worth mentioning that the SD fluctuations along FUT in Fig. 14(a) may originate from the presence of uneven strain due to the compact packing of fiber on to the mandrel.

Finally we also compare the time required by ANN, LCF and XCM for processing the BOTDA sensing signals after data acquisition. Since the training and testing phases of ANN are fully independent, we need to train an ANN only once to process the BGSs obtained at a particular scanning step. Thus the actual processing time using ANN can be considered as the running time in the testing phase only. To analyze the processing speed of the three techniques, the running time to process 10000 spectra for temperature profile extraction are recorded for using ANN, LCF and XCM, respectively. The ratio of running time using LCF to that using ANN is shown in Fig. 15(a), while the ratio of running time using XCM to that using ANN is depicted in Fig. 15(b). The results show that the processing speed using ANN is significantly faster than that using LCF or XCM, and the ratios increase at large frequency scanning step. This is because LCF requires more iteration to process the distorted BGSs acquired at such large scanning step and XCM needs more time for data interpolation to improve the frequency resolution. However, due to the less data acquired at large frequency

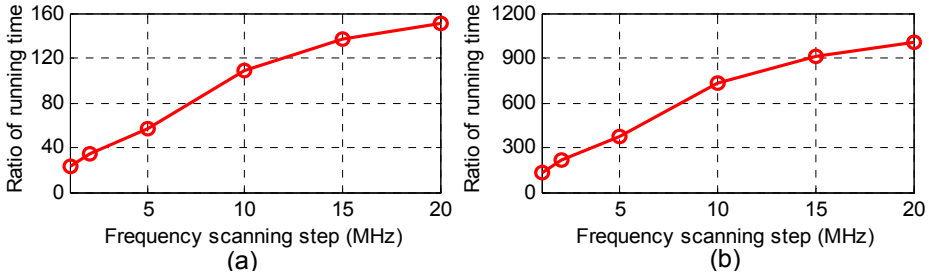

Fig. 15. Ratio of running time between (a) LCF and ANN and (b) XCM and ANN to process 10000 BGSs along the FUT after data acquisition.

scanning step, the time for data processing using ANN decreases exponentially as the scanning step increases. Therefore, by adopting large scanning step BOTDA systems using

#257807 Received 20 Jan 2016; revised 9 Mar 2016; accepted 9 Mar 2016; published 18 Mar 2016

ANN for temperature extraction can significantly reduce the measurement time but without degrading the performance when compared with those using LCF and XCM.

5. Conclusion

ANN has been successfully employed to extract temperature information along the fiber from the local BGSs measured by BOTDA. In the training phase, for each frequency scanning step a multi-layer feed-forward ANN is trained with ideal Lorentzian shaped BGSs with varying linewidth to take the linewidth variation of BGSs obtained from BOTDA measurements into account. The training phase helps ANN to acquire the knowledge on the pattern of the BGSs and corresponding temperatures before it is used in temperature extraction. While in the testing phase, the optimized ANN is applied to obtain the temperature information directly. The comparison of the performance between ANN and LCF or XCM shows that ANN can provide higher accuracy and greater tolerance to measurement noise, especially for the BGSs acquired from the BOTDA measurements at large frequency scanning steps. In addition, once the ANN has been trained, the processing speed using ANN is much faster than that using LCF and XCM. We believe that ANN would be a potential and alternative tool to extract temperature or strain information from the measured BGSs by BOTDAs, especially at large frequency scanning step for the significant reduction of the measurement time without sacrifice of accuracy.

Acknowledgments

Abul Kalam Azad thanks the Research Grants Council, Hong Kong for the financial support under the Hong Kong PhD Fellowship Scheme 2012/13 and Liang Wang thanks the financial support under The Hong Kong Polytechnic University Postdoctoral Fellowships Scheme 2015 (Project No. G-YW0S). The authors acknowledge the support of National Science Foundation of China (NSFC) under Grant No. 61377093, 61435006 and HK GRF grant PolyU 5208/13E.

#257807 Received 20 Jan 2016; revised 9 Mar 2016; accepted 9 Mar 2016; published 18 Mar 2016